MDPI

Article

Mechanism of Grain Densification in Nano- and Poly-Crystalline Cu Films and Its Impact in Advanced Metallization Processes

Brunella Cafra [1], Alessandra Alberti [2], Gaetano Calogero [2,*], Ioannis Deretzis [2], Antonio Landi [1], Daniele Pagano [1], Salvatore Sanzaro [1,2] and Antonino La Magna [2,*]

[1] STMicroelectronics, Stradale Primosole, 50, 95121 Catania, Italy; brunella.cafra@st.com (B.C.); antonio.landi@st.com (A.L.); daniele.pagano@st.com (D.P.); salvatore.sanzaro@st.com (S.S.)

[2] National Research Council, Institute for Microelectronics and Microsystems (IMM-CNR), VIII Strada 5, 95121 Catania, Italy; alessandra.alberti@imm.cnr.it (A.A.); ioannis.deretzis@imm.cnr.it (I.D.)

* Correspondence: gaetano.calogero@imm.cnr.it (G.C.); antonino.lamagna@imm.cnr.it (A.L.M.)

Abstract: We investigate the microstructural evolution of electrochemically deposited poly-crystalline Cu films during subsequent thermal process cycles at mild maximum temperatures, compatible with the integration in advanced metallization schemes for electronic device manufacturing. The modifications induced by the thermal budget have been characterized at different scales (from the film-substrate interface to the wafer scale) with different complementary techniques: X-ray Diffraction (XRD), scanning electron microscopy (SEM), atomic force microscopy (AFM), and dynamical warpage measurements. Moreover, the film internal grains' evolution has been modelled by a tri-dimensional on-cell model, derived by the Pott-like multi-states configurational energy dependence, able to consider multiple orientation of the grains and densification kinetics in the canonical ensemble. Finally, a macroscopic model of the warpage dependence on the process conditions is discussed. The presented joint theoretical and experimental analysis provides a complete and consistent scenario of the grain densification phenomenon and its impact for the Cu film microstructure and the composite system morphology, indicating several strategies for the integration of the process in real device structures.

Keywords: copper; metallization; annealing; warpage; polycrystalline; grain boundaries

Citation: Cafra, B.; Alberti, A.; Calogero, G.; Deretzis, I.; Landi, A.; Pagano, D.; Sanzaro, S.; La Magna, A. Mechanism of Grain Densification in Nano- and Poly-Crystalline Cu Films and Its Impact in Advanced Metallization Processes. *Crystals* **2024**, *14*, 125. https://doi.org/10.3390/cryst14020125

Academic Editor: Pavel Lukáč

Received: 15 December 2023
Revised: 19 January 2024
Accepted: 23 January 2024
Published: 26 January 2024

Copyright: © 2024 by the authors. Licensee MDPI, Basel, Switzerland. This article is an open access article distributed under the terms and conditions of the Creative Commons Attribution (CC BY) license (https://creativecommons.org/licenses/by/4.0/).

1. Introduction

The increasingly high capability and switching frequency in power electronic devices requires suitable metallization schemes, not only for electrical connection but also for dissipation of the thermal heat generated by the high power density [1,2]. In this respect, Cu metallization, with its increased electromigration resistivity, low resistivity (1.7×10^{-6} Ωcm) and high thermal conductivity (4.01 Wcm/K at 300) [3,4] is replacing the Al layer [5] currently in use, actively removing the thermal energy and preventing device damaging [3]. Furthermore, Copper front metal enables to consider Cu-Cu wire bonding, which offers alternatives to the Cu-Al or Au-Al systems.

However the application of a Cu-based metallization scheme requires an accurate control of the morphological evolution of nano- or poly-crystalline Cu film during the processing steps [6,7]. Indeed, despite the cited advantages, nearly room temperature electroplated copper has unstable grains, with a high density of defects such as impurities coming from bath, dislocations, and grain boundaries, which can be considered as the main source of a large amount of energy stored in the as-deposited fine grains of electroplated Cu films [4,5]. Therefore, the layer has to be thermally stabilized. Thermal treatment of thick Cu deposited on semiconductors' substrates modifies the composed system at different scales. For instance, Cu in direct contact with Si can lead to relevant kinetic reaction at relatively low temperature [8]. Moreover, micro-structural modifications in the Cu film, induced by the grain densification phenomenon, transfer a stress field in the

elasto-plastic regime to the substrate [9], which has a dramatic effect as global warpage of wafers.

A significant warpage makes power device fabrication difficult, especially if the final device thickness is lower than 100 µm. Moreover, high wafer warpage causes yield loss during chip assembly and package mount on the circuit board. Strategies aimed at warpage control and optimization enabling this challenging technology are hence necessary, implying a deeper understanding of the microscopic kinetics and global mechanical behaviour of the Cu-Si and, in general, Cu-substrate systems. From the macroscopic point of view, freestanding films and films deposited to thick substrates in fact behave differently. A noticeable difference is that freestanding films can be stressed only in tension whereas films bonded to substrates with relatively low coefficients of thermal expansion can be stressed in both tension and compression by varying the temperature. Furthermore, plastic deformation in a layer-substrate system bonded is, in some way, governed by the substrate [10].

A complete analysis of the impact of a metallization (sequence of depositions and thermal curing) to the micro- and macro-structures (metal layers, compliant interfaces, underlying substrates, global wafers) affected by the process is difficult to find in the literature. Therefore, the optimization of the processes' conditions is usually obtained without a comprehensive study of the micro-structural evolution for "all" the crystalline materials present in the system. Moreover, the support of reliable 3D models, simulating the system kinetics with the due accuracy, also seems very necessary in this kind of investigation.

In this work we provide an innovative holistic approach to the problem, exploring the micro-structural changes in electrochemically deposited (ECD) poly-crystalline Cu films during subsequent thermal cycles at moderate maximum temperatures, suitable for integration into advanced metallization schemes for electronic device manufacturing. The alterations resulting from the thermal treatments are analysed at various scales, ranging from the film-substrate interface to the wafer scale, using complementary techniques such as X-ray Diffraction (XRD), scanning electron microscopy (SEM), atomic force microscopy (AFM), and dynamical warpage measurements. First, we investigate 20 µm thick Cu layers grown by ECD on (from top to bottom) Cu 200 nm/(Ti)W 300 nm/Si substrates, highlighting the occurrence of self-annealing in the as-deposited samples, the grain densification due to thermal treatment and its impact on wafer warpage. A tri-dimensional (3D) on-cell model, based on the Pott-like multi-states configurational energy dependence, is also employed to simulate the internal grains' evolution in the films, while accounting for multiple grain orientations and densification kinetics in the canonical ensemble. Then, we compare samples with (hereafter named "Cu_{ECD}") and without (hereafter named "Cu_{seed}") the thick ECD-grown Cu layer on top, discussing the implications of thermal treatment on the morphology of the composite Cu/substrate system. In particular, we study how the interfacing Cu 200 nm/(Ti)W 300 nm stack mediates the interactions between the ECD-grown Cu layer and the rest of the substrate.

2. Materials and Methods

The Cu_{ECD} samples consist of 20 µm thick Cu layers grown by electrochemical deposition (ECD) on Cu 200 nm/(Ti)W 300 nm/Si substrates, with commercially available ENTHONE baths in an AMAT-RAIDER equipment (Santa Clara, CA, USA). The Cu_{seed} samples refer to the same systems but without the top Cu layer (i.e., prior to ECD). The (Ti)W and Cu 200 nm layers were sequentially PVD deposited on a (100) substrate using the AMAT-Endura-PVD system by introducing Ar in the PVD chamber and reaching the base pressure of about 7 mTorr. The sputtering power was 3.5 kW. The deposition time was 100 and 150 s, respectively, for Cu and (Ti)W. The intermediate (Ti)W layer is used as adhesion promoter layer. (Ti)W stands for a layer deposited by PVD using a TiW target with 90% wt W, 10% wt Ti. Therefore, we can consider the film as a W rich W-Ti system. The Cu 200 nm layer is a PVD deposited layer that can guarantee the Cu_{ECD} layer growth.

Without this layer the Cu_{ECD} does not nucleate and grow. The thicknesses of intermediate layers were chosen to guarantee film continuity and represent a good compromise in terms of induced warpage. Bulk thermal treatment in the temperature range between 150 °C and 400 °C has been performed on all samples. The annealing temperature cycles were implemented with up and down ramps at constant rates while the plateau was maintained for 60 min in all the cases. Warpage measurements have been performed by means of an MX 102-204-RA-2C tool by E+H Metrology GmbH (Karlsruhe, Germany). The warpage is defined as the maximum variation between individual points on the upper side of the wafer with respect to a least squares fit plane based on these points [11]. The stress of the as-deposited and thermally treated Cu_{seed} and Cu_{ECD} samples has been calculated by using Stoney's formula [12,13]. Morphology changes have been studied using SEM (DualBeam 865 by FEI Company, Hillsboro, OR, USA, in SEM modality) and AFM (Vx210 Atomic-Force Profiler by Veeco, Munich, Germany). Statistic of grain size distribution and evolution as a function of temperature has been obtained using several representative plan view SEM analyses. Structure and composition have been studied by X-ray Diffraction (XRD) analysis using an AXS D8 DISCOVER diffractometer by Bruker (Billerica, MA, USA) working with a Cu-Kα source.

The Cu_{ECD} grain densification has been simulated by means of a cellular automata-like approach (see, e.g., Ref. [14] and references therein) allowing a realistic description of the grains' evolution (growth). The kinetics are simulated by means of stochastic sequences of local transitions of the "cells" of a three dimensional lattice, where the poly-crystalline structure is mapped. The single cell represents a volume portion and stores the value of the orientation variable of the volume itself. The local event promoting the nano- or poly-crystal evolution (note that the size and resolution can be properly tuned, as it depends on the elementary cell volume) is the status change of the cells which can modify their orientation, at a given time $t0$ of the evolution, to another one among the total number N_{orien} of the possible ones. The corresponding transition probability (rate) is ruled by the local energy barrier ΔE, according to the transition state theory. The "potential" transition rate is

$$R = \begin{cases} \omega & \text{if } \Delta E \leq 0 \\ \omega \times exp\left[-\frac{\Delta E}{kT}\right] & \text{if } \Delta E > 0 \end{cases} \quad (1)$$

where ω is the only calibration parameter in the model and the energy barrier ΔE is calculated by the following Pott-like [15] lattice energy model

$$E(\theta_i) = J(\theta_i) \sum_{nn} [1 - \delta(\theta_i, \theta_{nn})], \quad (2)$$

where $\theta_i = \alpha, \beta, \gamma \ldots$ is the "orientation" of the volume in the i-th cell, $J(\theta_i)$ the grain boundary (monomer-grain) energy cost, θ_{nn} is the orientation of the next neighbour cell in the lattice and δ is the usual discrete delta function. We note that the energy in the bulk of the grain is the reference energy since $E(\theta_i) = 0$ for a cell which has all the neighbours with the same orientation. $J(\theta_i)$ is a calibration function which for homogeneous materials is chosen in a way that the model recovers the correct melting transition at the melting temperature T_M (see Figure 1). Moreover, by means of a fine tuning of $J(\theta_i)$, an orientation penalty, epitaxial or similar interface dependent energy modification could also be effectively included in the model for future extensions. The frequency ω has been chosen, aligning simulated and real kinetics in a single temperature process, then the same value is used for all the cases. Time integration in the Pott-like model is usually performed with the continuum time algorithm, which accelerates the computation [16].

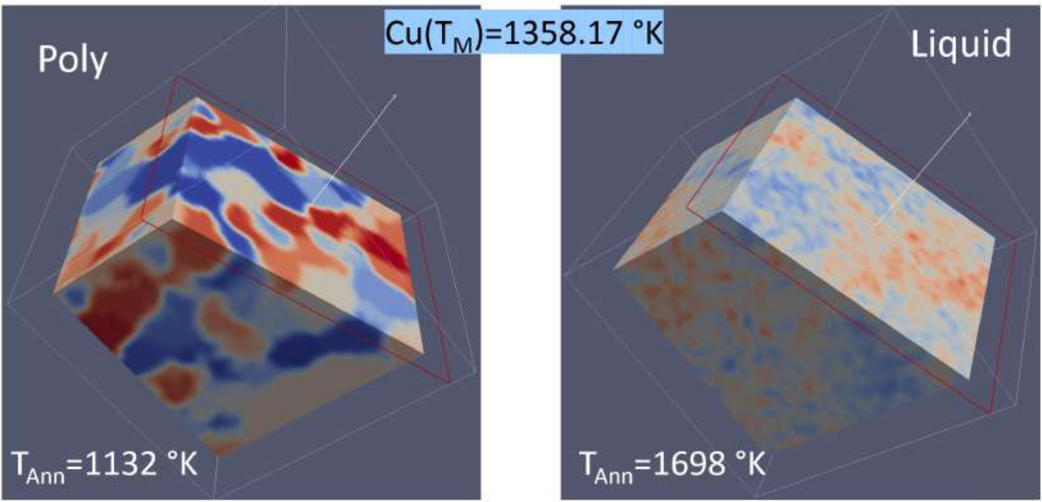

Figure 1. Poly-Cu volume simulated at the constant annealing temperatures indicated: below (**left** graph) and above (**right** graph) the melting point TM = 1358.17 K: the solid(poly)-liquid transition is recovered.

3. Results and Discussion

Stress values for Cu_{ECD} layers are shown in Figure 2. The as-deposited Cu layer has a stress value of about 18 MPa. After thermal annealing at 150 °C the stress value increases up to 47 MPa. Note that the Cu layer at this temperature is not stable and will evolve in terms of stress and layer morphology. Indeed, the stress value increases as a function of the annealing temperature, reaching a maximum value of 70 MPa at 220 °C. At temperature values higher than 220 °C the film stress decreases, reaching the minimum value of 56 MPa at 400 °C. The temperature dependence of stress represents a first indication of the structural changes that the system undergoes during the thermal annealing treatment.

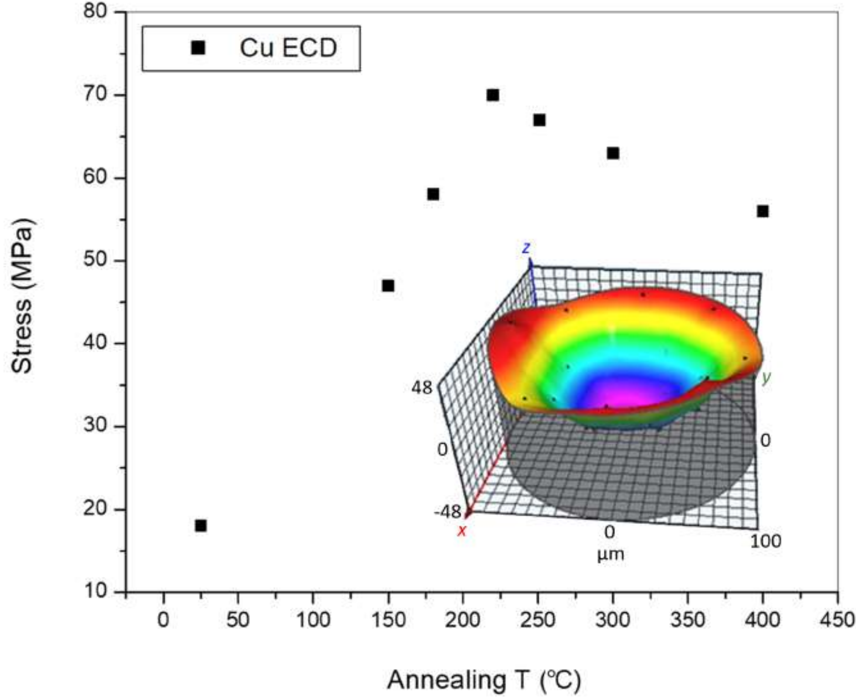

Figure 2. Stress as a function of annealing temperature for the Cu_{ECD} layer. An increase in stress with respect to the as-deposited layer is observed for values above 150 °C. For annealing temperature higher than 220 °C, a drop of stress value is observed.

To get insights on these modifications at the micro-scale, we have investigated the Cu_{ECD} morphological evolution correlating microscopic analysis Cu_{ECD} after the thermal curing and the full processes' simulations. Plane view SEM analyses and grain size distribution of Cu_{ECD} as-deposited and thermally treated at 180 °C, 250 °C and 400 °C are shown in Figures 3 and 4 respectively, and compared with the simulation results. All layers are dense and there is no observable porosity or cracks on the surface. Room temperature crystallization with the appearance of relative large Cu grains, termed self-annealing (SA), occurs in as-deposited samples (Figure 3, left side graphs). This state is reproduced in the simulation with a suitable long annealing at low T (50 °C) starting from a initial totally disordered state. We notice that the self-annealed state is used as the initial one in all the simulations of the curing processes after the verification that ±20% modifications in the preparing self-annealing simulation in terms of temperature and time does not significantly affect the results of the subsequent simulated Cu curing processes. In the experimental systems, the self-annealing is instead a consequence of the deposition mode (continuous DC mode) that allows for concurrent and progressive nucleation, grain growth, and recrystallization, while maintaining high deposition rates. This is a peculiarity of the DC mode with respect to the pulsed deposition (on-off) mode, where the grain nucleation occurs during the "on" time step whilst stress relaxation, grain growth and recrystallization occurs during the "off" time step.

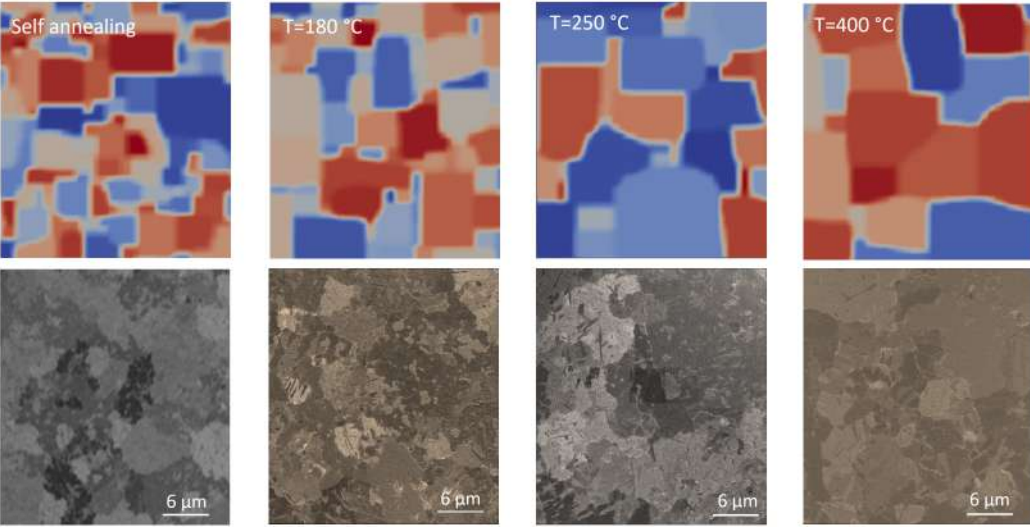

Figure 3. Comparisons with the same scale between surface grain morphology simulated (**top** panels) and real (**bottom** panel) cases. The simulated systems' size is $104 \times 104 \times 20\ \mu m^3$. All the processes are described in the text.

Reliable considerations can be derived by integrating SEM post-process analysis with kinetic simulations. In terms of final state description, they are in a significant agreement as the comparisons of the final snapshots and grain size distributions in the Figures 3 and 4 demonstrate. The use of the 3D simulations offers significant vantages in the study of the kinetics with respect to the theoretical scheme based on grain mean-size only [17,18], since the full size distribution can be properly modelled. We notice that, to align in parallel experiments and simulations, the snapshots in Figure 3 are shown within the same space scale and the statistical analysis in Figure 4 are performed with the same bin intervals of 2.25 µm width (coloured bars in left and right columns of Figure 4). The simulations are performed in a rather large simulation box ($104 \times 104 \times 20\ \mu m^3$) and the analysis can be extended in the whole three dimensional film structure, allowing for a more refined statistic of the size distribution (i.e., with a smaller bin), as the ones shown (with 0.45 µm bins' width) with the black line contours of the bars in the graphs reported in the left column of Figure 4. We notice that the combination of structural analysis and simulations indicates that, in spite of the non monotonic behaviour as a function of the temperature shown in

Figure 2, the Cu grain densification occurring at the micro-scale drives the stress behaviour at the wafer-level. The impact of the temperature on the ripening phenomenon is clearly evidenced by the simulations and validated by the experimental data. The driving force for the ripening is the reduction of the grain boundaries, due to their energetic cost with respect to the bulk, with a consequent global contraction of the film, no additional modification to the Pott model formulation is necessary to recover the experimental scenario. The simulations calculate a final reduction of the grain boundary volume of 55%, 41%, and 27% for the 180 °C, 250 °C, and 400 °C cases respectively with respect to the self-annealed post deposition state.

SEM microscopy shows that in thermally treated samples the huge increase in grain size and the induced deformation are associated with the formation of twin defects that are clearly visible for the three annealing temperatures (see, e.g., the arrows in Figure 3). Since no evidence of twinning has been detected on self-annealed samples, the twinning formation can be considered as a consequence of micro-state modification induced by the thermal treatment in our samples. This plastic release of the densification induced stress has also been reported by Simoes et al. [19] who observed the microstructural evolution of Cu grains during in situ annealing and showed that twins form inside a Cu grain, which grows extensively at the expense of other small grains.

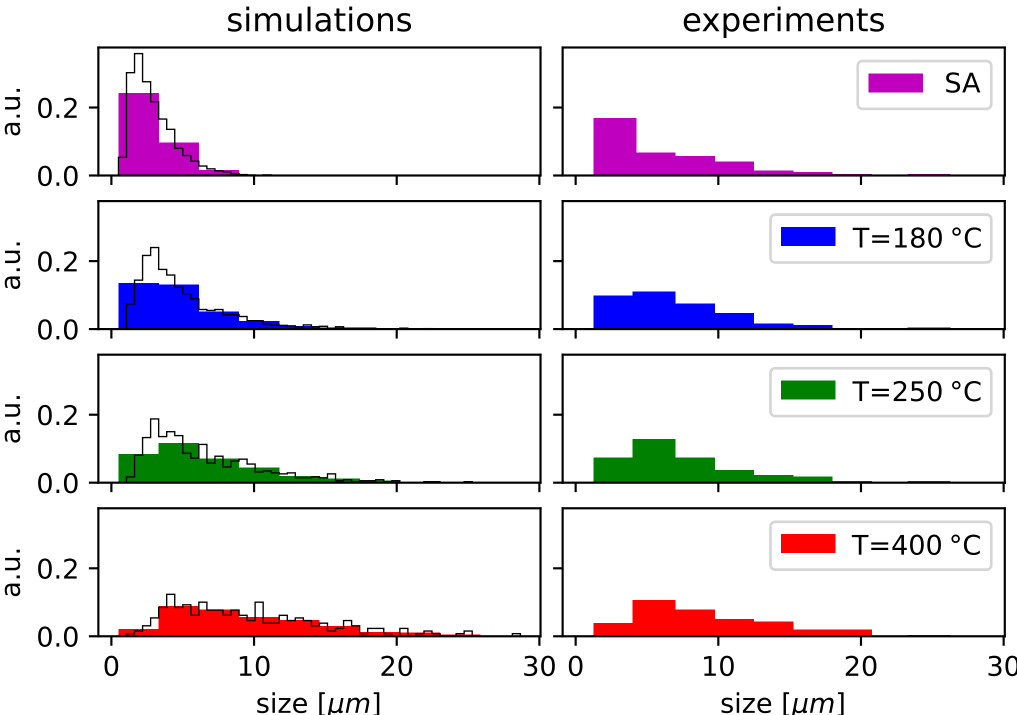

Figure 4. Comparisons between simulated grain size distributions (**left** panels) and the measurements ones (**right** panels). We notice that the simulated distribution are normalized to 1. The simulated systems' size is $104 \times 104 \times 20\ \mu m^3$. The thin black lines show the simulated distributions sampled using a larger number of bins. All the processes are described in the text.

Despite the similar grain size distribution, the layers exhibit quite a different surface roughness, such as the Rq value of 95 nm in case of annealing at 250 °C and of 28 nm in case of annealing at 400 °C (Figure 5). Another important feature highlighted by the AFM analysis is the Cu grain boundary, which appears well defined in the surface height map measurement only in case of annealing at 400 °C.

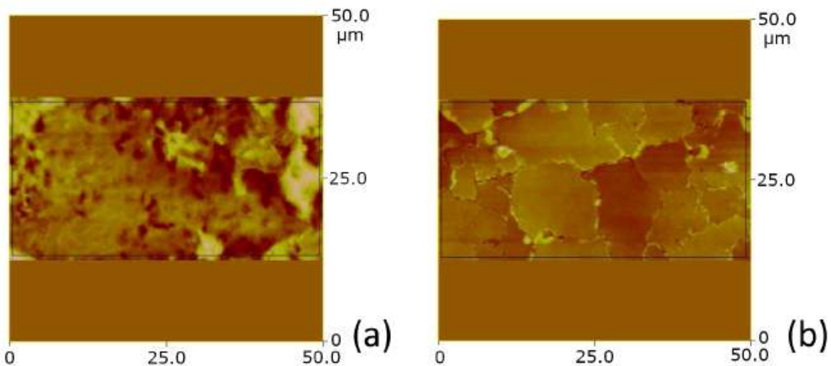

Figure 5. AFM images for samples annealed at 250 °C (**a**), and 400 °C (**b**).

While the grain evolution leads to a reduction of the grain boundary volume, which increases with the temperature, the stress trend in Figure 2 seems to indicate an important role of the Cu-film/Si-substrate interface. We have tried to understand the relationship between film evolution and global stress, investigating the micro-structural modifications of the interface stack without the presence of the 20 µm thick Cu film. Figure 6 shows stress values as a function of temperature for Cu_{seed} samples. The data are a mean value over several wafers intending to test process reproducibility. The deposited layers exhibit a quite large compressive stress of about −1.1 GPa. After thermal treatment, the stress values dramatically decreases down to −0.1 GPa with only slight changes as a function of annealing temperature. The figures on the inset report a wafer shape as obtained by the curvature measurement.

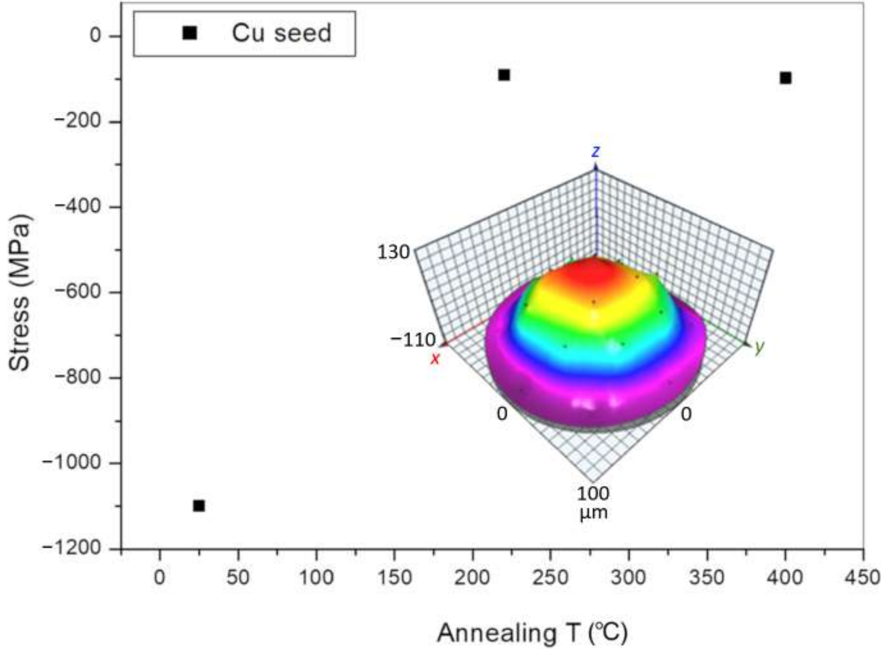

Figure 6. Stress as a function of annealing temperature for Cu_{seed} layers. An increase in stress with respect to the as-deposited layer is observed for the annealed samples.

Plan view SEM analyses and grain size distribution of Cu_{seed} as-deposited and thermally treated samples at 250 °C and 400 °C are shown in Figure 7. Pictures captured after Cu_{seed} deposition reveal a fine grained structure (Figure 7a) with the total frequency of grains at the side of the smaller dimension of the distribution: the grain dimensions not exceeding 200 nm and the median value being 100 nm (Figure 7b). After thermal treatment at 250 C grains with regular, square shaped faces with rounded edges start to appear (Figure 7c). These faces, oriented in various directions, extend deeper into the surface,

creating a cube-like pattern. The grain count dramatically decreases, the size distribution assuming a unimodal aspect (Figure 7d). An increase in median grain size up to 200 nm has been measured in this case. Only residual fine Cu seed grains can be appreciated at an annealing temperature of 400 °C (Figure 7e). Histogram populates towards the high grain dimension with an appearance of a bimodal distribution.

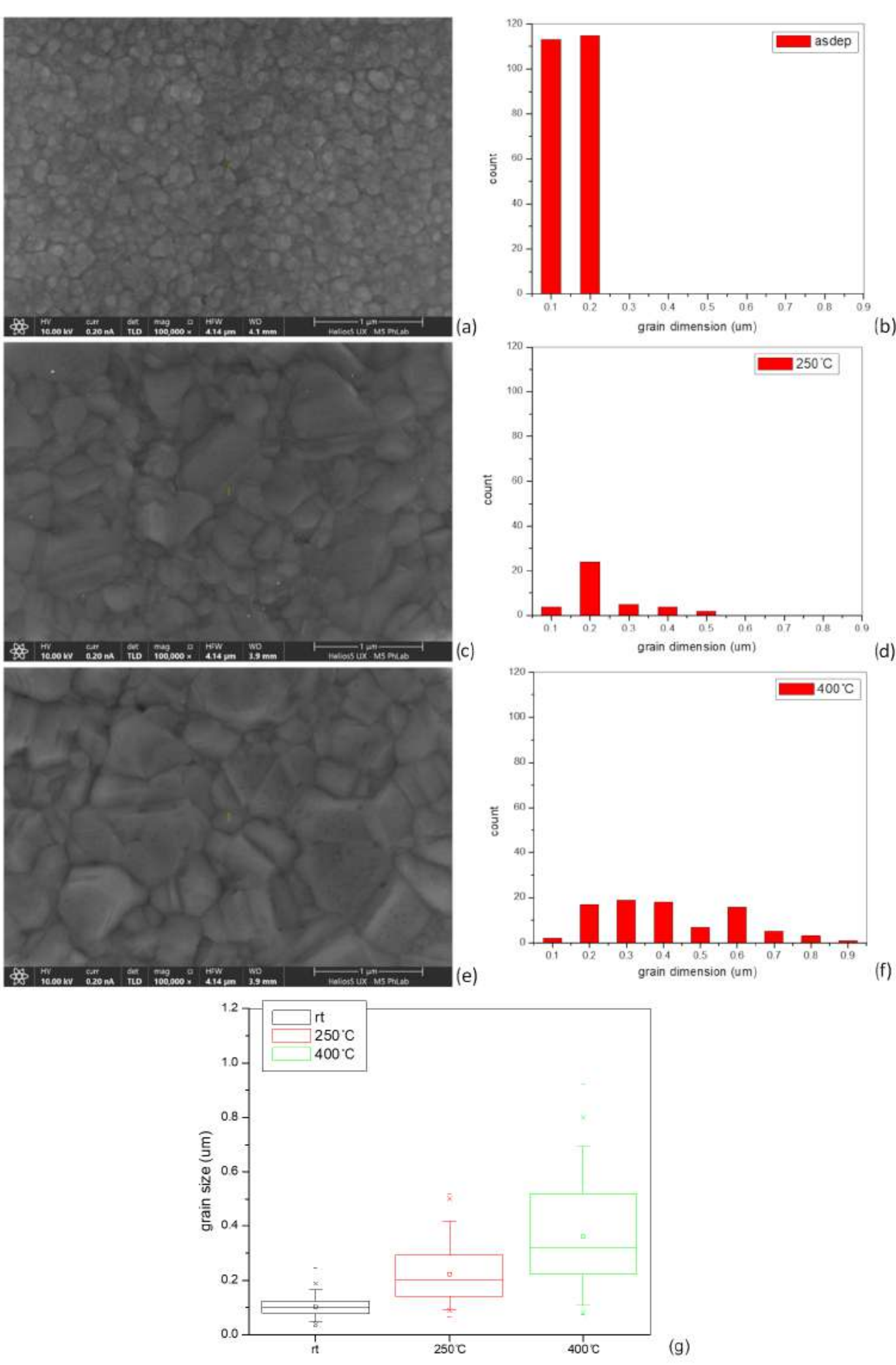

Figure 7. Microstructure of Cu_{seed} samples after deposition (**a**), 250 °C (**c**), 400 °C (**e**), and respective grain-size distribution (**b**,**d**,**f**). Box plot of grain sizes at different temperatures (**g**). The square marker represents the mean of the distribution; the × and dashed markers represent (from bottom to top) its 1st, 5th, 95th and 99th percentiles; the horizontal line within the box represents its median.

Surface roughness changes on a 10×10 μm^2 area are shown in Figure 8. An almost flat surface with Rq = 3.5 nm has been found on the as-deposited samples (Figure 8a). After the thermal treatment, the Rq value increases to 18 nm in the case of 250 °C (Figure 8b) and 20 nm in the case on 400 °C (Figure 8c).

To identify the structural modification that both Cu_{seed} and Cu_{ECD} samples undergo after thermal treatment at different temperatures, XRD analyses have been done in symmetric XRD configuration (see the top right inset of Figure 9). The XRD pattern of the entire Cu_{seed} sample in as-deposited conditions is shown in Figure 9. We can observe the different contributions of W (light blue line), (Ti)W (blue line), Cu (black line), and the other peaks related to the substrate. The schematic reported in the inset on the top left shows the sample structure, where we can observe the details regarding the layers' thickness. Concerning the Cu contributions, we found two out of the three main peaks of the Face-Cubic Centred (FCC) lattice, i.e., the (111) at 2θ = 43.35° and the (200) at 2θ = 50.48°. We note that other FCC peaks might exist outside the range of XRD angles explored in this work (i.e., 35–60°).

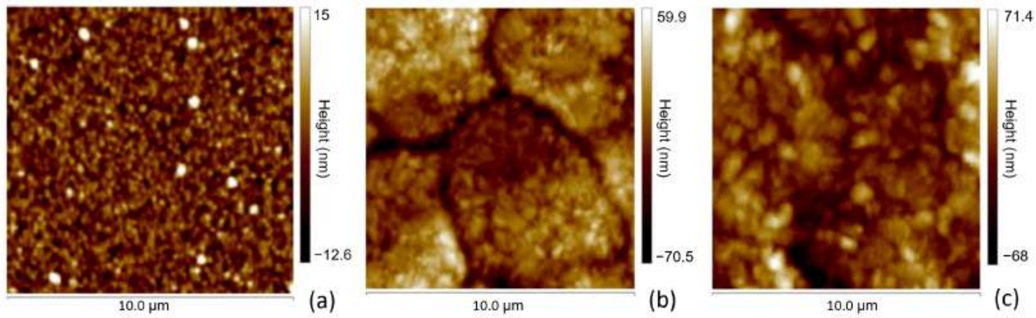

Figure 8. AFM images for Cu_{seed} samples as-deposited (**a**), annealed at 250 °C (**b**), and at 400 °C (**c**).

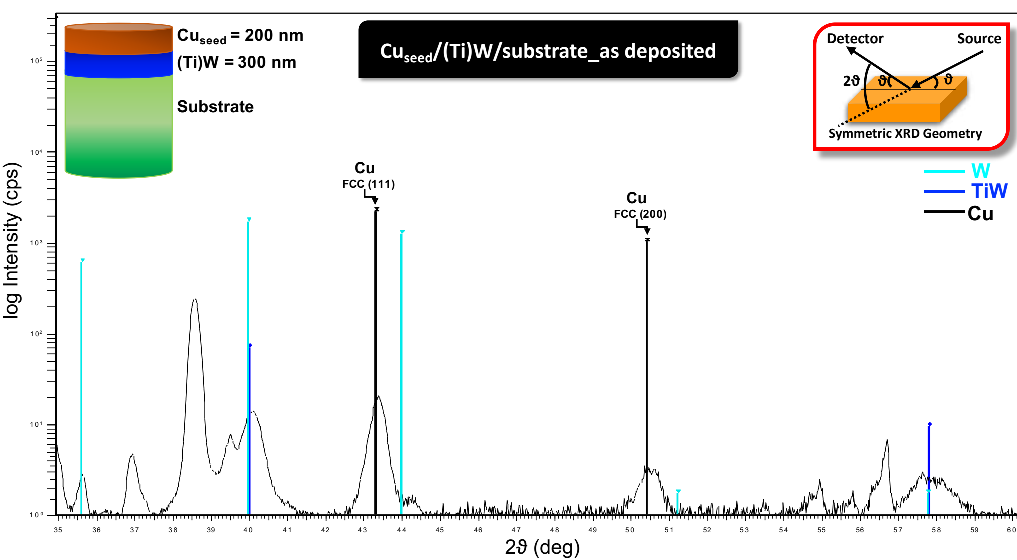

Figure 9. XRD pattern in symmetric configuration (top right inset) of the 200 nm Cu seed layer deposited on the substrate, as reported in the top left inset.

The Cu_{seed} sample has also been treated at different temperatures, i.e., at 250 °C and 400 °C, respectively. The purpose of these treatments was to verify how the temperature influences two important issues: (1) the improvement of the structural order and (2) a preferential orientation between the two Cu main peaks. Figure 10a shows the normalized area trend of the (111) Cu peak after thermal treatment at 250 °C and 400 °C compared to the as-deposited condition. The values increase with temperature, indicating an improvement of the structural order regarding the (111) Cu planes for the samples where the thermal budget was applied.

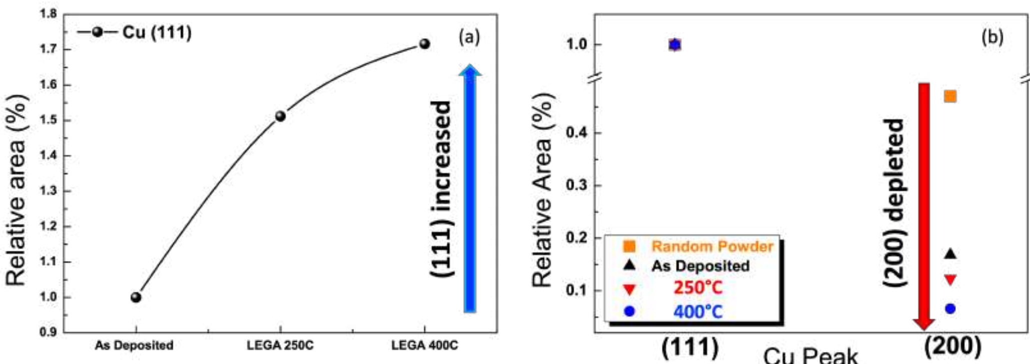

Figure 10. Relative area trend of the treated Cu_{seed} samples at 250 °C and 400 °C normalized to the as-deposited condition (**a**) of the (111) Cu peak and (**b**) the comparison between (111) and (200) Cu main peaks.

In order to have a complete scenario in terms of the structural properties for the Cu main peaks, we compared the relative area of the Cu (111) and (200) peaks with the Cu random powder sample as a reference. We found that the relative area ratio between the (111) and (200) Cu planes for each sample gradually decreased with increasing temperature (see Figure 10b).

Figure 11a shows the XRD patterns, in the range 2θ = 34–59°, for the Cu_{seed} samples in as-deposited conditions and with a thermal treatment both at 250 °C and at 400 °C. Here, we highlight with light blue the W peaks related to the (200), (210), and (310) planes located at the 2θ = 35.59°, 2θ = 39.97° and 2θ = 57.81°, respectively. The intensity trend of each peak in the three different conditions is reported in Figure 11b, where an intensity lowering is evident for all W peaks in the annealed samples. In particular, for the (200) and (310) W planes, the relative intensity value is the same for both Cu_{seed} samples treated at 250 °C and at 400 °C. On the other hand, for the W peak related to the (210) plane, we found a small difference between the two thermal budgets, likely because this plane is less sensitive to a soft thermal budget like 250 °C. Further details of the relative differences of the W peaks are shown in Table 1.

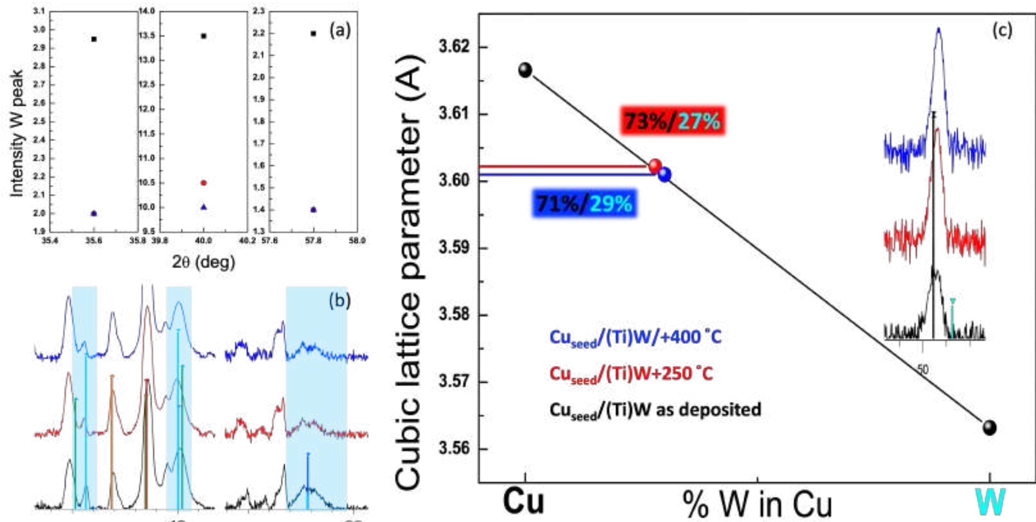

Figure 11. (**a**) XRD patterns, in the range 2θ = 34–59°, of the Cu_{seed} samples in as-deposited condition and with thermal treatment at 250 °C and at 400 °C; (**b**) intensity trend of the W peaks related to the light blue label shown in Figure 9; (**c**) Vegard plot of the XRD peak at 2θ = 50.45° (see inset).

Table 1. Relative differences of the intensity of W peaks after thermal treatment at 250 °C and 400 °C with respect to the as-deposited condition.

Plane	As-Deposited	@250 °C	@400 °C
(200)	2.95	2.00 (−33.2%)	2.00 (−33.2%)
(210)	13.5	10.5 (−23.2%)	10.0 (−26.9%)
(310)	2.20	1.40 (−37.3%)	1.40 (−37.3%)

Figure 11c shows a Vegard plot focused on the XRD peak at $2\theta = 50.45°$ (see inset). Following Vegard's law, if we assume that the lattice parameter of a Cu/W binary system changes linearly between the pure Cu and pure W lattice parameters, we can estimate the %W dispersion in the Cu matrix. Using this approach, we estimated the %W dispersed inside the Cu matrix for both Cu_{seed} samples thermally treated at 250 °C and 400 °C:

- Thermal treatment @250 °C → Cu/W − 73%/27%;
- Treatment @400 °C → Cu/W − 71%/29%.

Hence, we found an increase in %W within the Cu matrix after temperature annealing, which facilitates the dilution of W. It is worth noting that, although W and C are thermodynamically immiscible [20], our findings support the formation of Cu-W pseudo-alloy [21]. Indeed, diffusion and mixing phenomena occurring in thin film systems could lead to a metastable state that deviates from the equilibrium phase diagram.

To complete our structural analysis, we compared the Cu_{seed} and Cu_{ECD} samples. This final study was useful to understand if the two kinds of samples show different behaviours in terms of structural properties regarding the two Cu main peaks, i.e., the (111) and (200), respectively. Figure 12 schematically shows the analogies between the two samples concerning the lattice spacing ($d_{lattice}$) and the crystalline size. The detailed data are reported in Table 2. After the thermal treatment, both samples show a similar behaviour, despite the differences in terms of thickness and morphology.

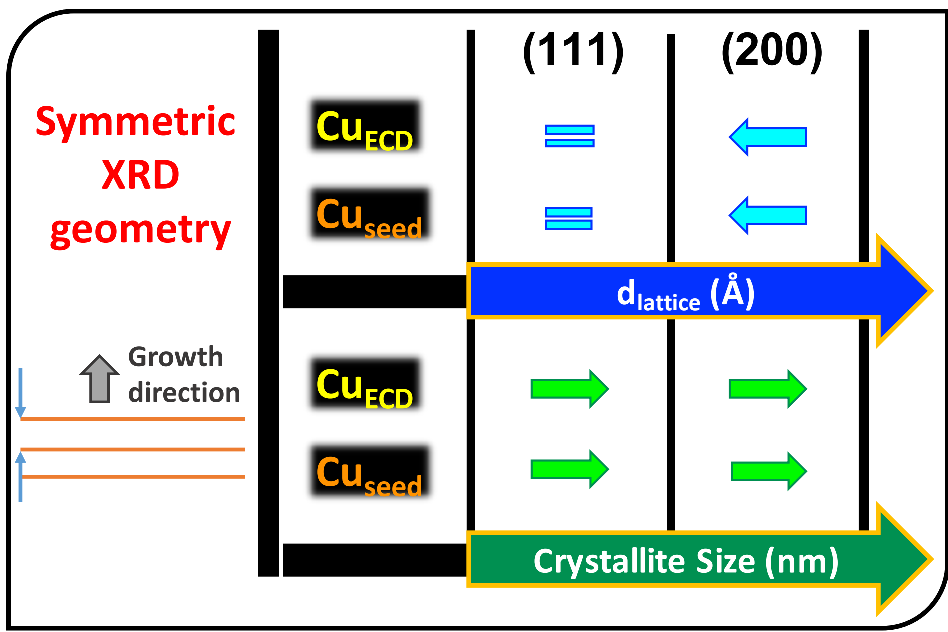

Figure 12. Schematized XRD comparison (referring to the data of Table 2) in terms of lattice spacing and crystalline size for Cu_{seed} and Cu_{ECD} samples. The Cu peaks are related to the (111) and (200) planes located at $2\theta = 43.34°$ and $2\theta = 50.44°$, respectively.

Table 2. Structural data comparison between the Cu_{seed} and Cu_{ECD} samples.

Sample	Plane	2θ (°)	d (Å)	Size (nm)	Δd/d (%)
ECD as dep.	(111)	43.340	2.0870	27.07	-
ECD @250 °C	(111)	43.340	2.0870	27.22	0.00
ECD @400 °C	(111)	43.340	2.0870	28.63	0.00
ECD as dep.	(200)	50.460	1.8080	24.95	-
ECD @250 °C	(200)	50.503	1.8065	25.36	−0.08
ECD @400 °C	(200)	50.496	1.8067	25.83	−0.07
seed as dep.	(111)	43.365	2.0859	20.91	-
seed @250 °C	(111)	43.365	2.0859	26.08	0.00
seed @400 °C	(111)	43.365	2.0859	26.54	0.00
seed as dep.	(200)	50.527	1.8057	12.61	-
seed @250 °C	(200)	50.597	1.8034	19.75	−0.13
seed @400 °C	(200)	50.648	1.8017	19.95	−0.22

4. Conclusions

The evolution of the electronic devices is guided by their functional design, which indicates new specifications for the sub-components of the device system. In the case of metal layers, new specifications could impact the feasibility of the processes' integration at different levels (scales), due to the modifications with respect to the standard necessary to obtain the desired results. Indeed, the metal deposition and the eventual further thermal curing could impact both the semiconductor micro- and nano-structures (inducing damage) and the subsequent processing (due, e.g., to an excessive global warpage of the wafer). Material science studies, eventually supported by process simulation, are necessary to deeply understand the phenomena involved in the process and speed up the integration procedure, also gaining predictive potential for future application of the methods in continuum improvement of the device performances.

In the present work, by combining several structural characterization techniques and in-cell 3D simulations, we have thoroughly investigated a process sequence aimed at increasing the ECD Cu film thickness with respect to those used in a previous device technology. Our results on the complete multi-layer stack Cu_{ECD} indicate that the driving force for the micro-structural evolution during the thermal cycle is the increase in grain size induced by a grain boundary-mediated ripening phenomenon. The simulations based on a properly calibrated Pott-like model predict with a good accuracy the internal kinetics of the poly-crystalline film for all the studied cases. Therefore, they represent a reliable tool for supporting the process development in different conditions and geometries.

Comparing the stress measurements at the wafer level for the full stack Cu_{ECD} and the partial stack Cu_{seed} (Figures 2 and 6) we conclude that the presence of the thick Cu film and its related evolution have a crucial impact at the wafer level: without the ECD process the stress has an opposite sign and a different trend with the temperature of the curing cycle. Moreover, the Cu_{ECD} wafer stress has a non-linear dependence on the cycle temperature. We have indicated two main phenomena concurring at this elasto-plastic behaviour: twin defects' formation and alloy redistribution at the interface. This redistribution is correlated to an improvement of the structural order after the thermal annealing. We could speculate that the non-linear stress behaviour is the composite effect of the grain densification and the interface rearrangement toward a more ordered state and a tighter bonding with the Si substrate. Actually the elastic (linear) thermal expansion must be considered to understand and model the stress evolution (see Ref. [9]). However, for our mild annealing cycle, the plastic deformations, induced by micro-structural changes (i.e., grains' densification), soon dominates the time dependence of the warpage during the thermal cycle. Elastoplastic models can in principle describe this time dependent trend, which could also lead to hysteresis [22], but they need suitable calibration. Future work will be dedicated to correlate grains' densification kinetics with this global wafer evolution.

We anticipate that further insights could be gained by means of complementary investigations based on the XRD $sin^2\psi$ method [23] or the focused ion beam digital image correlation (FIB-DIC) methodology [24]. Moreover, other techniques with better spatial resolution, such as the Electron Backscatter Diffraction (EBSD) [25], could complement XRD analyses of the thin Cu_{seed} samples.

These findings and, in general, the overall approach could be of strong interest for the optimization of this or similar processes, which is beyond the scope of the paper. Moreover, characterizations and simulations could be applied for the process design in the case of patterned systems. For the application to the metallization of nano-scaled devices the feature scale shrinks, however the methods can be expanded in terms of complexity and the accuracy of the analysis could also reach the atomic scale [26–28].

Author Contributions: Conceptualization, B.C., A.A. and A.L.M.; methodology, B.C., A.A. and A.L.M.; software, A.L.M.; validation, B.C., A.A., A.L., D.P., S.S. and A.L.M.; formal analysis, B.C., A.A., A.L., D.P., S.S. and A.L.M.; investigation, B.C., A.A., G.C., I.D., A.L., D.P., S.S. and A.L.M.; resources, B.C., A.A., A.L., D.P. and A.L.M.; data curation, B.C., A.A., A.L., D.P., S.S. and A.L.M.; writing—original draft preparation, B.C., I.D., A.A., A.L., D.P., S.S. and A.L.M.; writing—review and editing, B.C., A.A., G.C., I.D., S.S. and A.L.M.; visualization, B.C., A.A., G.C., I.D., A.L., D.P., S.S. and A.L.M.; supervision, B.C., A.A. and A.L.M.; project administration, B.C., A.A. and A.L.M.; funding acquisition, G.C. and A.L.M. All authors have read and agreed to the published version of the manuscript.

Funding: This research received no external funding.

Data Availability Statement: The data presented in this study are available on request from the corresponding authors.

Acknowledgments: This publication has been achieved in collaboration with the European Union—NextGenerationEU within the project PNRR "NFFA-DI" IR0000015-Missione 4, "Istruzione e Ricerca"—Componente 2, "Dalla ricerca all'impresa"—Linea di investimento 3.1, "Fondo per la realizzazione di un sistema integrato di infrastrutture di ricerca e innovazione"—Azione 3.1.1, "Creazione di nuove IR o potenziamento di quelle e sistenti che concorrono agli obiettivi di Eccellenza Scientifica di Horizon Europe e costituzione di reti".

Conflicts of Interest: The authors declare no conflict of interest.

References

1. Grujicic, D.; Pesic, B. Electrodeposition of copper: The nucleation mechanisms. *Electrochim. Acta* **2002**, *47*, 2901–2912. [CrossRef]
2. McCluskey, P. Reliability of Power Electronics under Thermal Loading. In Proceedings of the 2012 7th International Conference on Integrated Power Electronics Systems (CIPS), Nuremberg, Germany, 6–8 March 2012; pp. 1–8.
3. Nix, W.D. Mechanical properties of thin films. *Metall. Trans. A* **1989**, *20*, 2217–2245. [CrossRef]
4. Lagrange, S.; Brongersma, S.; Judelewicz, M.; Saerens, A.; Vervoort, I.; Richard, E.; Palmans, R.; Maex, K. Self-annealing characterization of electroplated copper films. *Microelectron. Eng.* **2000**, *50*, 449–457. [CrossRef]
5. Teh, W.; Koh, L.; Chen, S.; Xie, J.; Li, C.; Foo, P. Study of microstructure and resistivity evolution for electroplated copper films at near-room temperature. *Microelectron. J.* **2001**, *32*, 579–585. [CrossRef]
6. Lu, T.J.; Evans, A.G.; Hutchinson, J.W. The Effects of Material Properties on Heat Dissipation in High Power Electronics. *J. Electron. Packag.* **1998**, *120*, 280–289. [CrossRef]
7. Schmitt, R.P.; Menk, L.A.; Baca, E.; Bower, J.E.; Romero, J.A.; Jordan, M.B.; Jackson, N.; Hollowell, A.E. Void-free Copper Electrodeposition in High Aspect Ratio, Full Wafer Thickness through-Silicon Vias with Endpoint Detection. *J. Electrochem. Soc.* **2021**, *167*, 162517. [CrossRef]
8. Moiseenko, E.T.; Yumashev, V.V.; Altunin, R.R.; Zeer, G.M.; Nikolaeva, N.S.; Belousov, O.V.; Zharkov, S.M. Solid-State Reaction in Cu/a-Si Nanolayers: A Comparative Study of STA and Electron Diffraction Data. *Materials* **2022**, *15*, 8457. [CrossRef] [PubMed]
9. Chocyk, D.; Proszynski, A.; Gladyszewski, G. Diffusional creep induced stress relaxation in thin Cu films on silicon. *Microelectron. Eng.* **2008**, *85*, 2179–2182. [CrossRef]
10. Thompson, C.V.; Carel, R. Stress and grain growth in thin films. *J. Mech. Phys. Solids* **1996**, *44*, 657–673. [CrossRef]
11. E+H Metrology GmbH. *MX 102-204-RA-2C User Manual*; E+H Metrology GmbH: Karlsruhe, Germany, 2022.
12. Stoney, G.G. The tension of metallic films deposited by electrolysis. *Proc. R. Soc. Lond. Ser. Contain. Pap. Math. Phys. Character* **1909**, *82*, 172–175.
13. Freund, L.; Suresh, S. *Thin Film Materials. Stress, Defect Formation and Surface Evolution*; Cambridge University Press: Cambridge, UK, 2004.

14. Ullah, A.; Khan, M.; Weihua, X.; Hussain, S.; ur Rahman, M.; Salamat, N.; Haq, F. Simulations of grain growth in realistic 3D polycrystalline microstructures and the MacPherson–Srolovitz equation. *Mater. Res. Express* **2017**, *4*, 066502. [CrossRef]
15. Kim, Y.; Hwang, S.; Kim, M.; Kwun, S.; Chae, S.W. Three-dimensional Monte-Carlo simulation of grain growth using triangular lattice. *Mater. Sci. Eng. A* **2005**, *408*, 110–120. [CrossRef]
16. La Magna, A.; Coffa, S. Accelerated Monte Carlo algorithms for defect diffusion and clustering. *Comput. Mater. Sci.* **2000**, *17*, 21–33. [CrossRef]
17. Lu, L.; Tao, N.; Wang, L.; Ding, B.; Lu, K. Grain growth and strain release in nanocrystalline copper. *J. Appl. Phys.* **2001**, *89*, 6408–6414. [CrossRef]
18. Huang, J.; Zhang, J.; Cuevas, A.; Tu, K.N. Recrystallization and grain growth in bulk Cu and Cu (Sn) alloy. *Mater. Chem. Phys.* **1997**, *49*, 33–41. [CrossRef]
19. Simões, S.; Calinas, R.; Vieira, M.; Vieira, M.; Ferreira, P.J. In situ TEM study of grain growth in nanocrystalline copper thin films. *Nanotechnology* **2010**, *21*, 145701. [CrossRef] [PubMed]
20. Romano-Brandt, L.; Salvati, E.; Le Bourhis, E.; Moxham, T.; Dolbnya, I.P.; Korsunsky, A.M. Nano-scale residual stress depth profiling in Cu/W nano-multilayers as a function of magnetron sputtering pressure. *Surf. Coatings Technol.* **2020**, *381*, 125142. [CrossRef]
21. Wang, Y.; Zhuo, L.; Yin, E. Progress, challenges and potentials/trends of tungsten-copper (WCu) composites/pseudo-alloys: Fabrication, regulation and application. *Int. J. Refract. Met. Hard Mater.* **2021**, *100*, 105648. [CrossRef]
22. Sumarac, D.; Knezevic, P.; Dolicanin, C.; Cao, M. Preisach Elasto-Plastic Model for Mild Steel Hysteretic Behavior-Experimental and Theoretical Considerations. *Sensors* **2021**, *21*, 3546. [CrossRef]
23. Baczmanski, A.; Lark, R.; Skrzypek, S. Application of Non-linear Sin$^2\psi$ Method for Stress Determination Using X-ray Diffraction. In Proceedings of the Residual Stresses VI, ECRS6, Coimbra, Portugal, 10–12 July 2002; Materials Science Forum; Trans Tech Publications Ltd.: Bäch, Switzerland, 2002; Volume 404, pp. 29–34.
24. Sebastiani, M.; Eberl, C.; Bemporad, E.; Pharr, G.M. Depth-resolved residual stress analysis of thin coatings by a new FIB–DIC method. *Mater. Sci. Eng. A* **2011**, *528*, 7901–7908. [CrossRef]
25. Pereloma, E.; Edmonds, D.V. *Phase Transformations in Steels*; Woodhead Publishing Series in Metals and Surface Engineering; Woodhead Publishing: Sawston, UK, 2012; Volume 1.
26. Calogero, G.; Deretzis, I.; Fisicaro, G.; Kollmuß, M.; La Via, F.; Lombardo, S.F.; Schöler, M.; Wellmann, P.J.; La Magna, A. Multiscale Simulations for Defect-Controlled Processing of Group IV Materials. *Crystals* **2022**, *12*, 1701. [CrossRef]
27. Calogero, G.; Raciti, D.; Acosta-Alba, P.; Cristiano, F.; Deretzis, I.; Fisicaro, G.; Huet, K.; Kerdilès, S.; Sciuto, A.; La Magna, A. Multiscale modeling of ultrafast melting phenomena. *npj Comput. Mater.* **2022**, *8*, 36. [CrossRef]
28. Raciti, D.; Calogero, G.; Ricciarelli, D.; Anzalone, R.; Morale, G.; Murabito, D.; Deretzis, I.; Fisicaro, G.; La Magna, A. Multiscale atomistic modelling of CVD: From gas-phase reactions to lattice defects. *Mater. Sci. Semicond. Process.* **2023**, *167*, 107792. [CrossRef]

Disclaimer/Publisher's Note: The statements, opinions and data contained in all publications are solely those of the individual author(s) and contributor(s) and not of MDPI and/or the editor(s). MDPI and/or the editor(s) disclaim responsibility for any injury to people or property resulting from any ideas, methods, instructions or products referred to in the content.